Vibrational Circular Dichroism and Theoretical Study of the Conformational Equilibrium in (−)-S-Nicotine

ARTICLE *in* CHEMPHYSCHEM · NOVEMBER 2014

Impact Factor: 3.42 · DOI: 10.1002/cphc.201402652

3 AUTHORS, INCLUDING:

J. J. López González
Universidad de Jaén
134 PUBLICATIONS **1,138** CITATIONS

ChemPubSoc Europe

DOI: 10.1002/cphc.201402652

CHEMPHYSCHEM Articles

Vibrational Circular Dichroism and Theoretical Study of the Conformational Equilibrium in (−)-*S*-Nicotine

Pilar Gema Rodríguez Ortega, Manuel Montejo,* and Juan Jesus López González[a]

We report an extensive study of the molecular and electronic structure of (−)-*S*-nicotine, to deduce the phenomenon that controls its conformational equilibrium and to solve its solution-state conformer population. Density functional theory, ab initio, and molecular mechanics calculations were used together with vibrational circular dichroism (VCD) and Fourier transform infrared spectroscopies. Calculations and experiments in solution show that the structure and the conformational energy profile of (−)-*S*-nicotine are not strongly dependent on the medium, thus suggesting that the conformational equilibrium is dominated by hyperconjugative interactions rather than repulsive electronic effects. The analysis of the first recorded VCD spectra of (−)-*S*-nicotine confirmed the presence of two main conformers at room temperature. Our results provide further evidence of the hypersensitivity of vibrational optical activity spectroscopies to the three-dimensional structure of chiral samples and prove their suitability for the elucidation of solution-state conformer distribution.

1. Introduction

(−)-*S*-Nicotine is the main alkaloid present in tobacco leaves; the alkaloid extract from tobacco leaves contains approximately 90% (−)-*S*-nicotine.[1] It is also the main psychoactive ingredient in tobacco and is responsible for the addictive nature of tobacco smoking, which is one of the most widespread causes of premature death, heart disease, cancer, and respiratory disorders in the world.[2]

The psychoactive effects of nicotine (e.g. diminution of anxiety and stress levels, increased energy, euphoria, and improvement of cognitive functions) are the main appeals of smoking.[3,4] However, nicotine also acts as a potent agonist of the nicotinic acetylcholine receptor (nAChR),[5,6] which is a key neurotransmitter of the central and peripheral nervous system,[7] and has an inhibitory effect in cardiac tissue resulting in heart-rate lowering.[8]

Nicotinic agonists and antagonists of nAChR have been identified as therapeutic targets for the treatment of numerous diseases including Parkinson's disease; Tourette's syndrome; anxiety, cognitive, and attention deficits; and smoke addiction.[5–10] Regarding the treatment of Parkinson's disease (PD), it has been demonstrated that nicotinic compounds provide an excellent alternative to L-DOPA therapy,[9] because the latter is well-known to cause dyskinesias.[11] In contrast, nicotine can effectively facilitate movement and enhance and stimulate motor coordination in people with PD.[9] Additionally, (−)-*S*-nicotine has been found to evoke dopamine release, thus confirming the fact that it likely contributes to the neuropharmacological effects of nicotine and tobacco use.[12] Thus, a deep understanding of the molecular and electronic structures, and the conformational and electronic properties of (−)-*S*-nicotine and related compounds is essential to elucidate the nature and magnitude of their interactions with the biological targets, which will determine their biological role, and also for the subsequent design of new structurally related drugs. Consequently, (−)-*S*-nicotine has attracted the attention of many researchers, and, hence, several studies can be found in the literature concerning this system. These works are mainly focused on the theoretical study of the structure, preferred conformations, gas-phase basicity, and preferred protonation sites (either gas phase or solution) for nicotine and protonated nicotine.[13–20]

Among the most recent theoretical works concerning this system, two studies deserve special allusion. Yoshida et al. have recently published a comprehensive theoretical conformational analysis for nicotine, nornicotine, and their protonated species; the gas-phase conformations, barrier heights, and protonation states of these two systems were assessed by using ab initio calculations.[21] Barone et al. have carried out the evaluation of their self-developed software for computing vibrational optical activity (VOA) spectra of biomolecules by employing (−)-*S*-nicotine as a benchmark.[22] The anharmonic IR and vibrational circular dichroism (VCD) spectra in gas phase and in solution for (−)-*S*-nicotine were calculated using DFT calculations (B3LYP/aug-N07D). However, as they pointed out, their study lacked a direct theoretical–experimental comparison, because the VCD spectra of (−)-*S*-nicotine had not been reported in the literature at that date.

Regarding experimental studies of this system, the first works focused on the spectroscopic analysis of nicotine date from the 1950s. FTIR spectroscopy, Raman spectroscopy, Fourier transform microwave spectroscopy, and gas-electron diffraction have been applied to the study of the molecular structure, conformations, and protonation states of nicotine and related

[a] *P. G. R. Ortega, Prof. M. Montejo, Prof. J. J. L. González*
Department of Physical and Analytical Chemistry
University of Jaén, 23071 Jaén (Spain)
E-mail: mmontejo@ujaen.es

Supporting Information for this article is available on the WWW under http://dx.doi.org/10.1002/cphc.201402652.

compounds.[23–29] The chiroptical version of Raman spectroscopy (i.e. Raman optical activity) has been recently applied to study (−)-*S*-nicotine in a water solution and indicated the presence of the two lower energy conformers in the low-frequency region.[27]

Despite the fact that the structural and molecular properties of the title compound have been the subject of several investigations, in our opinion there is still a lack of information required to answer some queries, such as the mechanisms governing the conformational equilibrium in this kind of species, and the possible incidence of intramolecular hydrogen bonding as a structural stabilizing feature in the minimum-energy conformers of (−)-*S*-nicotine, as suggested elsewhere.[21]

In the present study, to provide better insight into the phenomena governing the conformational changes and associated barriers heights and steric effects in this kind of species, we have carried out a joint theoretical and experimental investigation to elucidate the conformational landscape of (−)-*S*-nicotine in both the gas phase and solution state. We report, to the best of our knowledge, the first VCD spectra of (−)-*S*-nicotine, both for the pure liquid and in a range of solvents of increasing polarity; the thorough analysis of which has yielded spectroscopic evidence in the mid-frequency region of the contribution of its two main conformers in condense phases, and has shown the valuable discriminating potential of VCD in this regard. Furthermore, in spite of the existence of several theoretical works dealing with nicotine, we report the first systematic conformational search based on DFT and molecular mechanics methodologies performed for this system.

We believe that our work may be valuable for future studies focused on the interactions of this and other structurally related alkaloids with specific biological targets, and could potentially be applied in the design and development of new drugs for the treatment of the abovementioned diseases.

Experimental Section

Experimental Procedure

(−)-*S*-nicotine was purchased from Sigma–Aldrich and used without further purification. Mid-IR and VCD spectra of (−)-*S*-nicotine were recorded for the neat liquid and solutions in CCl_4 and dimethylsulfoxide (DMSO). The mid-IR and VCD spectra of (−)-*S*-nicotine were recorded by using a JASCO FVS-4000 FTIR spectrometer, equipped with an indium antinomide detector (4000–1900 cm^{-1}) and a mercury–cadmium–telluride (MCT) detector (2000–900 cm^{-1}) detectors, and employing standard liquid cells and BaF_2 windows. In general, the spectra were recorded in the 2000–900 cm^{-1} range, by using a spectral resolution of 4 cm^{-1}, 2000 scans, and the MCT detector of the instrument. For the DMSO solutions, the spectral range was set to 2000–1100 cm^{-1} instead, owing to the presence of intense bands of the solvent below 1100 cm^{-1} that made it difficult to measure the VCD spectra of our target. The concentrations of the sample solutions were optimized to get the optimum absorbance range for the VCD and IR measurements of the samples. Thus, solutions with concentrations ranging from 0.5 to 2 M and cell path lengths of approximately 5–50 μm were employed as recommended in the literature.[30,31] Specifically, we used path lengths of 6 μm for recording the IR/VCD spectra of the pure liquid (−)-*S*-nicotine and concentrations of 1–2 M together with path lengths of 50 μm for recording the vibrational spectra of solutions in a nonpolar solvent (CCl_4). This methodology yielded IR absorbances in the 0.12–0.9 range . The spectra for solutions in a polar solvent (DMSO) were recorded by using concentrations ranging from 0.5–3 M together with path lengths of 6 μm (IR absorbances 0.6–0.8 were typically achieved). Baseline corrections were accomplished by subtracting the spectrum of the pure solvent recorded under the same experimental conditions from the spectrum of the sample; for the neat liquid, the spectrum for the empty cell was used.

Theoretical Methods.

The conformational search for (−)-*S*-nicotine was carried out by means of molecular mechanics (MM) calculations using the MMFF[32–36] and SYBYL[37] force fields as implemented in SPARTAN08 program package.[38] As (−)-*S*-nicotine is a heterocyclic alkaloid, and given that performing a systematic molecular mechanics conformer distribution exploration may lead to spurious structures, a Monte–Carlo method was employed instead. Further geometrical optimizations of the selected nonredundant conformers found by MM calculations and the computation of their harmonic vibrational frequencies with DFT and ab initio methods were performed using the Gaussian 09 (Revision D.01) suite of programs.[39] Geometry optimization criteria were SCF = tight and Int = Ultrafine. The Becke's three-parametric hybrid exchange functional[40] combined with the Lee–Yang–Parr correlation functional[41] and with the exchange component of Perdew and Wang's 1991 functional[42–44] (i.e. B3LYP and B3PW91 hybrid functionals) in conjunction with the 6-311++G**[45] and aug-cc-pVTZ[46] basis sets were implemented. B3LYP was chosen as it is considered as standard model chemistry for many applications and has been proven to yield accurate results for the study of thermochemical and spectroscopies properties in a wide range of molecular systems. The B3PW91 functional was chosen following recommendations given by Stephens and co-workers.[47] Their studies of a wide variety of medium-to-large size organic compounds pointed to the better performance, in general, of hybrid H-GGA functionals, and, in particular, of the B3PW91 and B3P86 functionals for the computation of VCD intensities in terms of mean absolute deviation values and the number of incorrect (±) peaks assigned (compared to experimental) in the computed VCD spectra. The second-order Möller–Plesset perturbation theory (fullMP2)[48] in conjunction with the 6-31G* and 6-31+G* basis sets[49,50] have also been used to validate minima and structures. Natural Bond Orbital (NBO)[51] calculations were accomplished using the program NBO v.6.0.[52] AIM calculations, based on Bader's theory, were performed using AIM2000 program.[53,54] Given that the solvents used for the experimental measurement of vibrational adsorption and VOA spectra are unlikely to form any strong hydrogen-bonding interactions with the system investigated here, we treated the solvent by applying integral equation formalism (IEF) version of the continuum PCM solvation model. Thus, solvent calculations were carried out according to the polarizable continuum model (IEF-PCM),[55–59] by using the dielectric constant values corresponding to CCl_4, DMSO, and D_2O, as implemented in Gaussian 09.

2. Results and Discussion

2.1 Conformational Landscape and Theoretical Molecular Structure of (−)-*S*-Nicotine

2.1.1 Gas Phase

Multiple conformers of (−)-*S*-nicotine are believed to contribute to the IR and VCD spectra of the molecule. As calculated spectra depend heavily on molecular conformations, a thorough conformational study is needed to perform a deep analysis of its vibrational spectra.

The conformational landscape of (−)-*S*-nicotine has been analyzed in two different ways: 1) by means of a "direct" DFT conformational search and 2) by performing molecular mechanics calculations.

"Direct" refers to the fact that the conformational search was accomplished taking into account the expected structures to be found following chemical intuition, that is, considering all the sources of flexibility in the molecule:

1) The arrangement of the pyrrolidine ring.
2) The N–CH_3 arrangement with respect to the ring plane (*endo* = opposite side of the pyridine ring or *exo* = same side of the pyridine ring).
3) The relative pyrrolidine–pyridine orientation (A or B).
4) The *cis* or *trans* configuration of the molecule.

A schematic picture of the twelve different molecular conformations considered is shown in Figure 1. After optimization at a moderate level of theory (B3LYP/6-31 + G*), those conformations comprising the half-chair arrangement of the pyrrolidine ring were discarded (third row in Figure 1). The nonexistence of negative vibrational frequencies (at the same theoretical level) confirmed the remaining eight optimized structures (envelope conformations) as real minima on the potential energy surface (PES) of (−)-*S*-nicotine.

To perform a more comprehensive analysis of the conformational landscape of (−)-*S*-nicotine (and also to confirm the internal consistency of the "direct" DFT search described above), MM conformational searches were carried out using both MMFF and SYBYL force fields. The parameters needed to expand the conformational search of the target were selected to ensure eclipsed conformations, envelope, boat, and half-chair conformations of the pyrrolidine ring were found. This conformer distribution analysis also yielded a total of eight molecular structures, which match those already found by means of the direct search. Furthermore, increasing the basis set size led to us discarding the m06 conformer (Figure 2), for which an imaginary frequency, corresponding to the torsional normal mode τC2C3C4C5 (see Figure 3 for atom numbering), was calculated (using the B3LYP and B3PW91 functionals, in conjunction with the 6-311++G** and aug-cc-pVTZ basis set, and at the MP2/6-31 + G* level). Consequently, only the remaining seven conformers were considered for subsequent analyses. Their B3LYP/aug-cc-pVTZ optimized structures are depicted in Figure 2.

Table 1 shows the more meaningful calculated geometrical parameters of the seven conformers of (−)-*S*-nicotine at the

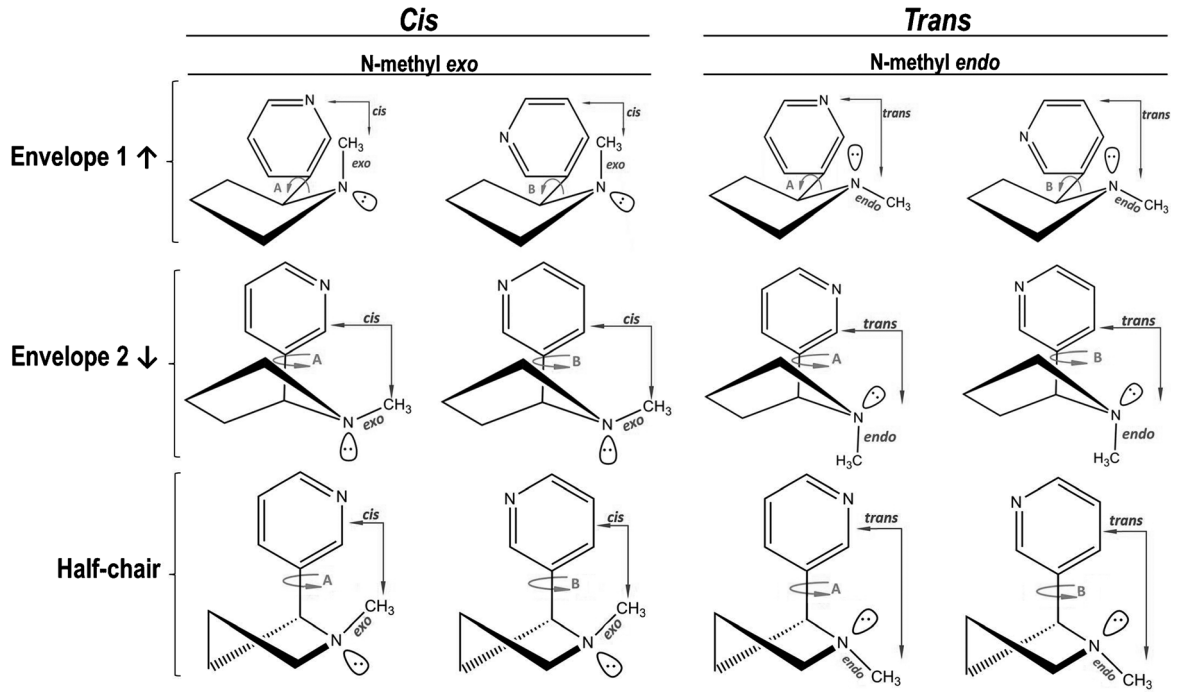

Figure 1. Schematic description of the conformers considered in the conformational search for (−)-*S*-nicotine. Possible ring puckering of the pyrrolidine ring, the *endo* or *exo* arrangement of the N-methyl group, the *cis* or *trans* configuration of the system, and the relative orientation of pyridine ring with respect to the pyrrolidine ring (i.e. rotational isomerism A or B) were all considered. The A and B labels represent for the two possible orientations of the pyridine ring with respect to the pyrrolidine-ring plane (rotational isomers). Half-chair structures turned into envelope structures, once the geometrical optimization was completed.

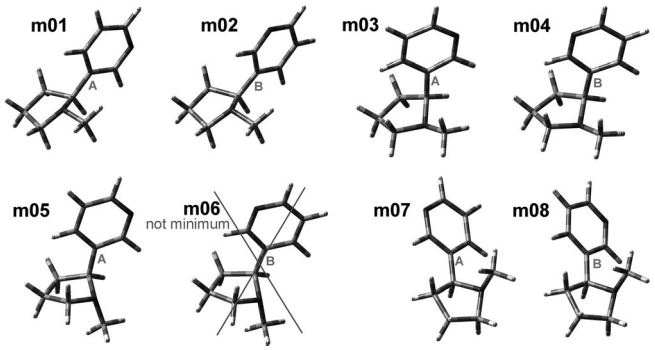

Figure 2. Optimized structures of the conformers found for the (−)-*S*-nicotine molecule at the B3PW91/aug-cc-pVTZ level of theory.

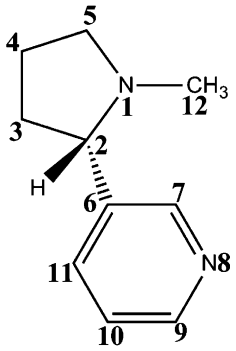

Figure 3. Molecular structure and atom numbering used for (−)-*S*-nicotine.

different levels of theory employed (see Figure 3 for atom numbering). As shown, all the optimized structures have a ϕC2C3C4C5 dihedral angle close to 0° (i.e. the pyrrolidine ring conformation is envelope-like for all the optimized conformers). It can be seen how conformers of (−)-*S*-nicotine are related in pairs, that is, the geometry of the m01 and m02 conformers mainly differ only in the relative position of the pyridine ring with respect to the pyrrolidine ring. The same goes for m03 and m04, and m07 and m08. Within the whole set of conformers, the ϕC2C3C6C7 dihedral angle can adopt two different values depending on whether the pyridine ring is an A or B arrangement: for A conformers ϕC2C3C6C7 is in the range −100 to −150° and for B conformers ϕC2C3C6C7 is about 70 to 10°.

In a recent study concerning gas-phase isomers of nicotine,[21] a classification of its conformers was made by considering two parameters according to the pseudorotation scheme[60] of the pyrrolidine ring in (−)-*S*-nicotine and the χ dihedral angle. Conformers m01, m02, m03, m04, m07 and m08 correspond to those labeled as (*W*,*trans*,*syn*), (*W*,*trans*,*anti*), (*E*,*cis*,*syn*), (*E*,*cis*,*anti*), (*W*,*cis*,*syn*), and (*W*,*cis*,*anti*), respectively, in Ref. [21]. Most of our conformers match those in Ref. [21], although conformer m05 is not considered in their study. Moreover, with our double strategy of conformational search we have not found the (*S*,*cis*,*syn*) and (*S*,*cis*,*anti*) conformers mentioned in Ref. [21]. To corroborate or discard the existence of these two conformers, we performed the optimization of these structures at the MP2/6-31+G* level.

Although the (*S*,*cis*,*anti*) conformer at the MP2/6-31G** level (used in Ref. [21]) may be a real minimum, the increase of the basis set size allowed us to discard this structure that, remarkably, has a pseudo half-chair arrangement of the pyrrolidine ring, similar to the conformers that we discarded after our "direct" DFT conformational search at the B3LYP/6-31+G* level, as mentioned above. In addition, taking the structure of the (*S*,*cis*,*syn*) conformer as starting point, our optimization at the MP2/6-31+G* level led to a different structure, which resembled our m03 conformer. Therefore, we highpoint the importance of including diffuse functions into the basis sets used for studying systems where delocalization effects are likely to happen, as otherwise the orbital space of the molecule won't be well described, leading to virtual stable configurations of the system.

The results regarding relative energies and Boltzmann's populations obtained with the four methods used (Table 2) only slightly differ, all of them point to the higher stability of the m01 and m02 conformers in the gas phase; these conformers account for 99.9% of the total sample composition in gas phase (m01 ≈ 70% and m02 ≈ 30%, B3PW91/aug-cc-pVTZ). As mentioned above, the main geometrical difference between the m01 and m02 conformers of (−)-*S*-nicotine is the relative position of the pyridine ring.

To find the stabilizing effect that is responsible for the greater stability of conformer m01 versus m02, we performed a NBO study (MP2/6-31+G*) of their electronic structures. We calculated the Lewis and non-Lewis energies of this pair of conformers. The first arises from deleting all the non-Lewis orbitals (i.e. Rydberg and starred orbitals) from the NBO basis set, hence calculating the idealized Lewis structure's energy of the systems. The non-Lewis energy is calculated by the summation of all intramolecular donor–acceptor interactions to

Table 1. Main geometrical parameters calculated at the B3LYP and B3PW91 level in conjunction with the 6-311++G** and aug-cc-pVTZ basis sets for a set of (−)-*S*-nicotine conformers.

Dihedral angle	m01	m02	m03	m04	m05	m07	m08	m01	m02	m03	m04	m05	m07	m08
	B3LYP/6-311++G**							**B3LYP/aug-cc-pVTZ**						
ϕC2C3C4C5	−1.3	−1.4	−6.0	−5.7	−3.6	8.5	8.4	−0.1	−0.3	−6.0	−5.7	−2.4	8.6	8.6
ϕN1C2C5C3	138.5	138.5	−138.4	−138.4	−142.4	137.4	137.7	138.2	138.2	−138.8	−138.7	−143.1	137.5	137.7
ϕC12N1C2C5	125.7	125.9	−132.9	−132.9	122.7	−120.9	−121.4	125.8	126.0	−133.3	−133.3	123.0	−121.2	−121.7
ϕC3C2C6C7	−104.5	74.9	−142.2	38.5	−159.6	−6.9	178.6	−105.9	73.5	−141.5	38.8	−156.8	−5.5	−179.3
	B3PW91/6-311++G**							**B3PW91/aug-cc-pVTZ**						
ϕC2C3C4C5	−1.0	−1.1	−5.8	−5.5	−3.6	8.0	7.7	0.48	0.16	−5.5	−5.3	−4.2	8.0	7.8
ϕN1C2C5C3	137.9	137.9	−137.7	−137.7	−142.4	137.1	137.3	137.5	137.6	−138.1	−138.0	−141.3	137.2	137.4
ϕC12N1C2C5	125.4	125.7	−132.1	−132.1	122.9	−120.3	−120.8	125.4	125.7	−132.6	−132.5	122.3	−120.5	−120.9
ϕC3C2C6C7	−103.8	75.6	−143.9	36.9	−159.6	−9.3	175.2	−105.4	74.2	−143.1	37.2	−163.6	−8.5	176.4

Table 2. Relative energies (kcal mol^{-1}) and Boltzmann's populations (% Pop.) calculated in gas phase at 298.15 K for (−)-*S*-nicotine set of conformers.[a,b]

	ΔG	% Pop.	ΔE_0	% Pop.	ΔG	% Pop.	ΔE_0	% Pop.
	B3LYP/6-311++G**				**B3PW91/6-311++G****			
m01	0.00	68.32	0.00	69.30	0.00	69.78	0.00	70.05
m02	0.46	31.63	0.48	30.60	0.50	30.16	0.51	29.83
m03	4.58	0.03	4.22	0.06	4.59	0.03	4.12	0.07
m04	4.76	0.02	4.38	0.04	4.78	0.02	4.27	0.05
m05	7.19	0.00	7.21	0.00	7.44	0.00	7.01	0.00
m07	7.28	0.00	6.85	0.00	7.09	0.00	6.55	0.00
m08	7.38	0.00	7.10	0.00	7.23	0.00	6.83	0.00
	B3LYP/aug-cc-pVTZ				**B3PW91/aug-cc-pVTZ**			
m01	0.00	66.85	0.00	68.63	0.00	67.23	0.00	69.15
m02	0.42	33.09	0.47	31.28	0.43	32.72	0.48	30.75
m03	4.51	0.03	4.25	0.05	4.56	0.03	4.21	0.06
m04	4.73	0.02	4.43	0.04	4.78	0.02	4.39	0.04
m05	7.07	0.00	7.22	0.00	6.96	0.00	7.17	0.00
m07	7.21	0.00	6.89	0.00	7.05	0.00	6.62	0.00
m08	7.27	0.00	7.11	0.00	7.12	0.00	6.84	0.00

[a] ΔE_0 ($E_0 = Ee + ZPE$) is the zero point corrected relative energy. [b] The theoretical population is calculated using the Boltzmann equation and taking $T = 298.15$ K.

give the energy lowering derived from all stabilizing hyperconjugative electronic delocalizations in the structure. The differences between the values calculated for m01 and m02 gave us an idea of the main phenomenon governing the conformational preference and stability of the m01 and m02 conformers of (−)-*S*-nicotine.

The difference in the Lewis energy between the two conformers is given by $\Delta E_L = E^L_{m01} - E^L_{m02} = 1.1$ kcal mol^{-1}, whereas the difference in the non-Lewis energy is given by $\Delta E^{NL} = E^{NL}_{m01} - E^{NL}_{m02} = 1.68$ kcal mol^{-1}. As expected, the $\Delta E^L + \Delta E^{NL}$ value matches the difference in the SCF energy between both conformers at the MP2/6-31+G* level. As shown, the localized energy contribution (Lewis energy) favors conformer m02 by 1.11 kcal mol^{-1}, whereas the stabilizing electronic delocalizations are greater for conformer m01 by 1.68 kcal mol^{-1}. It can be inferred that hyperconjugative effects tip the conformational equilibrium towards m01, which is the global minimum. Yoshida and co-workers[21] conjectured that the incidence of an intramolecular hydrogen bond in the structure of (−)-*S*-nicotine may be the cause of the energy difference between the two main conformers. However, given that the distances of the plausible intramolecular CH···N hydrogen bonds for m01 and m02 are 2.73 Å and 2.70 Å (B3PW91/aug-cc-pVTZ), respectively, and considering the stabilizing nature of such an interaction, it is contradictory that the m02 conformer is the less stable when it has a shorter (and presumably stronger) intramolecular hydrogen bond. Indeed, our efforts to theoretically characterize that interaction were unsuccessful using both, NBO and AIM calculations; the NBO didn't plot any electronic delocalization from the lone pair orbital of N(1) towards the σ^* orbital of the C(11)–H(16) bond, and the AIM method didn't locate any bond critical point (BCP) between these atoms (MP2/6-31+G* and B3PW91/aug-cc-pVTZ).

2.1.2. Solution

Theoretically determined relative energies and Boltzmann populations for the different conformers of (−)-*S*-nicotine in solution (CCl_4, $\varepsilon = 2.2$; DMSO, $\varepsilon = 46.8$; D_2O, $\varepsilon = 78.1$) reveal that, as in the gas phase, only the m01 and m02 structures would significantly contribute to the total sample composition (approximately 99.9%). Data collected in Table 3 also indicate that the energy profile of (−)-*S*-nicotine conformers is not strongly medium dependent, that is, relative energies barely change when going from gas phase to solution states in solvents of increasing polarity. Even in polar solvents, that is, DMSO and D_2O, the m01/m02 ratio is similar to that calculated in the gas phase (approximately 2:1).

Table 3. Relative energies (kcal mol^{-1}) and Boltzmann's populations (% Pop.) calculated in solution (CCl_4, DMSO and D_2O) at 298.15 K for conformers m01 and m02 of (−)-*S*-nicotine.[a,b]

	B3LYP/aug-cc-pVTZ				B3PW91/aug-cc-pVTZ			
	ΔG	% Pop.	ΔE_0	% Pop.	ΔG	% Pop.	ΔE_0	% Pop.
	CCl_4							
m01	0.00	67.06	0.00	67.84	0.00	65.90	0.00	67.60
m02	0.42	32.88	0.44	32.05	0.39	34.03	0.44	32.28
	DMSO							
m01	0.00	62.44	0.00	63.04	0.00	56.92	0.00	61.89
m02	0.30	37.47	0.32	36.81	0.17	42.99	0.29	37.94
	D_2O							
m01	0.00	62.29	0.00	62.82	0.00	57.13	0.00	61.79
m02	0.30	37.62	0.31	37.03	0.17	42.79	0.29	38.04

[a] ΔE_0 ($E_0 = Ee + ZPE$) is the zero point corrected relative energy. [b] The theoretical population is calculated using the Boltzmann equation and taking $T = 298.15$ K. Note that only m01 and m02 conformers are depicted in this table, as these are the only populated structures in both the gas phase and solution. Relative energies obtained for the minor conformers in solution, have been taken into account when computing Boltzmann' populations for (−)-*S*-nicotine.

With regards to the molecular structures of the m01 and m02 conformers, small differences can be addressed by comparing their main geometrical parameters in gas phase and in solution (CCl_4, DMSO and D_2O). To exemplify this, similarity analyses of the corresponding molecular geometries were accomplished by using the Vega ZZ program[61–63] to yield low root-mean-square (RMS) deviation values: 0.002 (m01 gas-CCl_4), 0.006 (m02 gas-CCl_4), 0.013 (m01 gas-DMSO), 0.009 (m02 gas-DMSO), 0.013 (m01 gas-D_2O), and 0.010 (m02 gas-D_2O). Molecular structures superimposition images depicted in Figure S1–S3 (see the Supporting Information) account for this.

The fact that the polarity of the solvent does not noticeably alter either the structure or the theoretical Boltzmann distribution of the main conformers of (−)-*S*-nicotine supports our NBO results above. This indicates the dominant role of hyperconjugative delocalization as the driving force to control the conformational equilibrium in this species, rather than electrostatic interactions between polar groups or bonds, because, in that case, larger effects in the calculated populations of m01 and m02 (and the remaining conformations) would be expected.

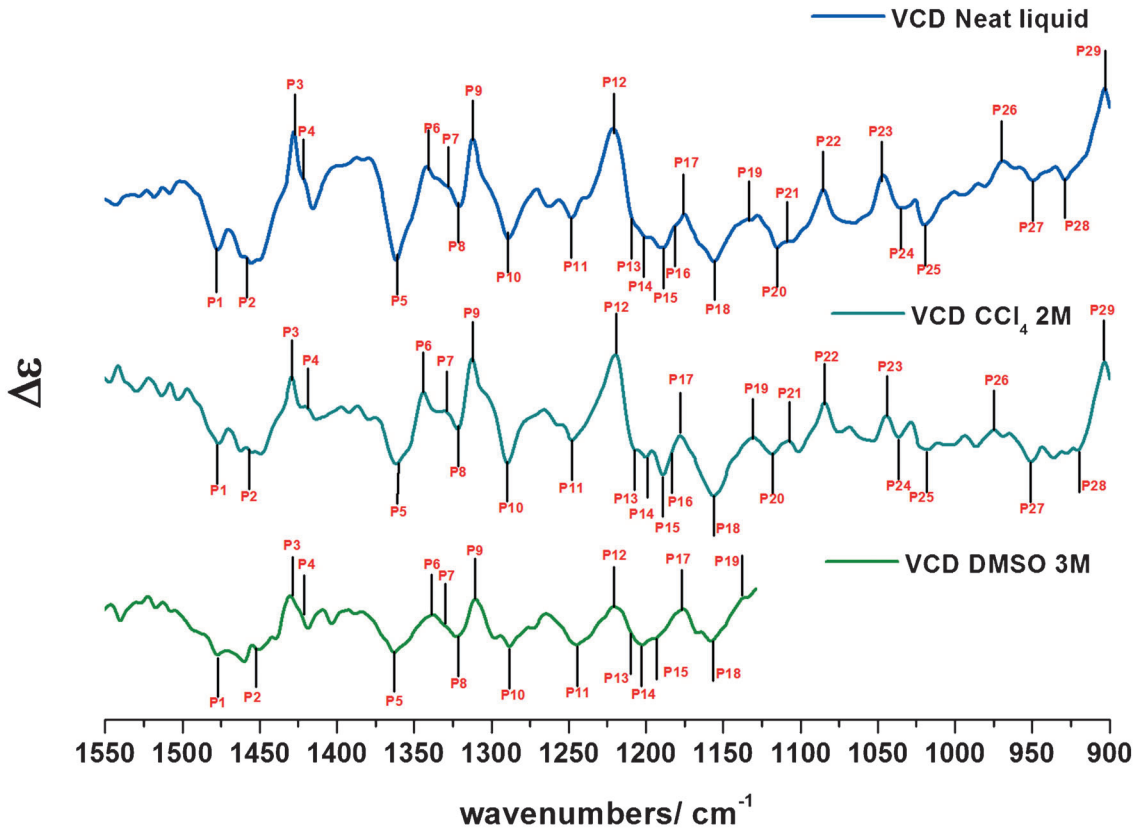

Figure 4. Experimental VCD spectra of (−)-*S*-nicotine in the 1550–900 cm^{-1} region for the neat liquid (pathlength 6 μm ;top) and for a CCl_4 2 M solution, (pathlength 50 μm; middle) and in the 1550–1125 cm^{-1} region for a DMSO 3 M solution (pathlength 6 μm; bottom).

2.2 Determination of the Conformer Distribution of (−)-*S*-Nicotine by Vibrational Spectroscopy: FTIR and VCD

Figures 4 and 5 show the VCD and IR spectra of neat (−)-*S*-nicotine and its CCl_4 solutions (in the 1550–900 cm^{-1} region), and DMSO solutions (in the 1550–1125 cm^{-1} region). Although we had also carried out calculations in water solutions, the use of water as a solvent was discarded, because: 1) the intrinsic difficulty of using it as solvent both for IR and VCD measurements and 2) the slight solvent effect in calculated conformer populations and molecular geometries, which would presumably prevent the observation of remarkable differential features in the spectra. For the sake of clarity, in Figure 4 and 5, all the experimental bands have been marked and labeled numerically. Note that the VCD spectra have been taken as reference for numbering (the number of experimental VCD bands is higher than the observed IR bands that have been labeled accordingly).

As shown, the IR and VCD spectral profiles obtained with CCl_4 as the solvent are similar to those observed for the neat liquid, whereas the spectra with DMSO show some subtle differences in the position and relative intensities of the bands observed in certain regions, which are more evident in the case of the VCD spectrum (see for example peaks P12, P15, P17, and P18 in Figure 4). This is a clear example of how highly polar solvents may interact strongly with the sample and affect its chiroptical response in solution, and thus, must be used carefully. In contrast, the relative intensities of the IR bands in DMSO solution are barely affected and solvent effects (although also present) are less noticeable in this case (see peaks P12, P15, P17, and P18 in Figure 5).

As stated above, we chose the B3PW91 functional to perform the structural study of (−)-*S*-nicotine, because it has been suggested to be a reliable method for computing VCD intensities and wavenumbers of an extensive variety of systems.[30] Nonetheless, we have found that, in our case, the B3LYP functional yields better results. This is illustrated in Figure S4–S6 (see the Supporting Information), where we show comparisons between the experimentally recorded VCD spectra of the sample (neat liquid, and CCl_4 and DMSO solutions) and the theoretical Boltzmann-averaged spectra using the relative energies calculated both B3LYP/aug-cc-pVTZ and B3PW91/aug-cc-pVTZ in gas phase and under the IEF-PCM model. Although, the experimental spectra are fairly well-reproduced by both methods, B3LYP provides better results than B3PW91 both in terms of the shape of the calculated spectral profile (especially in the 1250–1150 cm^{-1} region, where, as discussed below, the presence of the two main conformers in the sample can be detected) and also in terms of the accuracy of the calculated wavenumbers (theoretical–experimental deviations). Thus, we considered the B3LYP/aug-cc-pVTZ data for the vibrational analysis. The experimental wavenumbers of the bands marked in Figure 4 and 5, together with the corresponding theoretical wavenumbers (B3LYP/aug-cc-pVTZ), calculated rotational

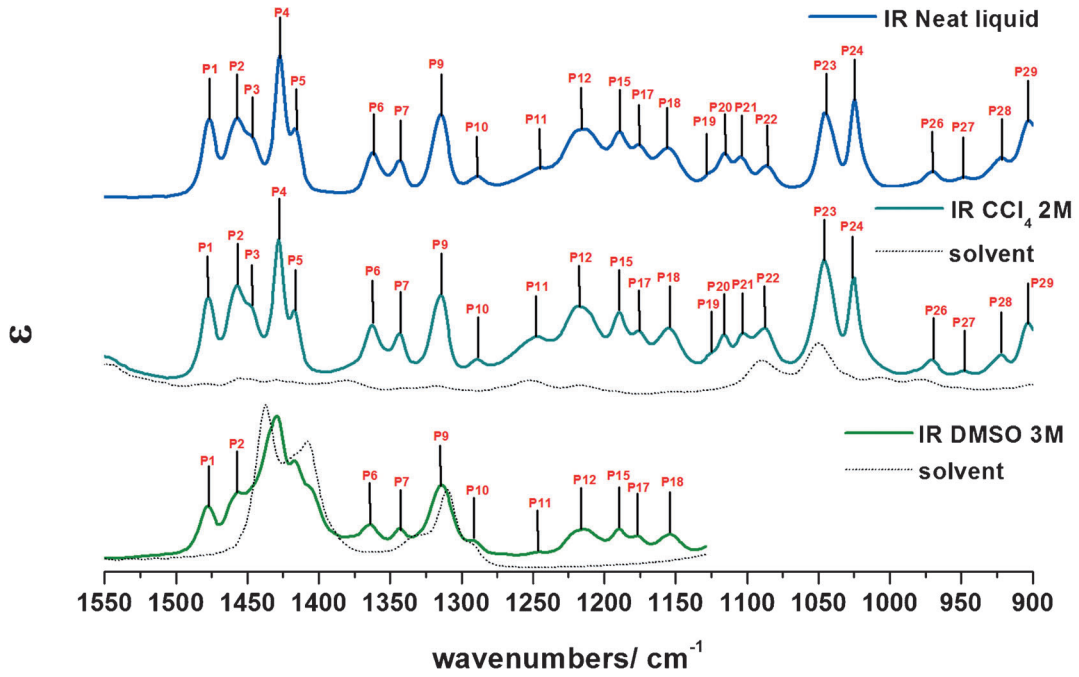

Figure 5. Experimental IR spectra of (−)-*S*-nicotine in the 1550–900 cm^{-1} region for the neat liquid (pathlength 6 μm; top) and for CCl_4 2 M solution (pathlength 50 μm; middle) and in the 1550–1125 cm^{-1} region for DMSO 3 M solution (pathlength 6 μm; bottom).

strengths (R_i), and their vibrational assignment are collated in Table 4.

As shown in Figure 4 and 5, a total of 29 bands (neat liquid and CCl_4 solution) are observed in the measured region of the VCD spectra, whereas only 25 of these bands are seen in the same region of the corresponding IR spectra. This finding indicates the higher sensitivity of the VCD technique to the three-dimensional structure of (−)-*S*-nicotine and is proof of the extra discriminating potential of this technique. Moreover, our theoretical calculations (B3LYP/aug-cc-pVTZ) predict that a total of 35 peaks should appear between 1500 and 900 cm^{-1} as shown in Table 4.

Notably, only 14 out of the 35 theoretical peaks in the 1500–900 cm^{-1} region can be set as robust normal vibrational modes (NMVs) when strictly following the criteria adopted in Refs.[64,65] regarding the ξ angle (i.e. angle formed between the electric transition dipole moment and magnetic transition dipole moment vectors for a given normal mode). In any case, the calculated theoretical wavenumbers for the NMVs that have been assigned to peaks P11–P17 appearing in the 1250–1150 cm^{-1} region (i.e. the region employed for carrying out the conformational discrimination as discussed below) are mostly robust, which proves the consistency of the vibrational analysis and the assignment carried out in the present work (see Table S1 in the supporting Information).

Figures 6 and 7 show the theoretical–experimental comparison of the VCD and IR spectra of (−)-*S*-nicotine. As shown, the Boltzmann-averaged spectral profiles calculated using the relative ΔG energies (67% m01 and 33% m02) are in fairly good agreement with the experimental spectra. This good match between theory and experiment allow the features appearing in the 1500–900 cm^{-1} frequency region to be unambiguously assigned to the $\delta_{ip}CH$ and $\delta_{ip}CC$ of pyridine ring, the ρCH_2, τwCH_2 and $waCH_2$ of pyrrolidine ring, the $\delta^{as}CH_3$, $\delta^{s}CH_3$ of the N–CH_3 group, and the $\nu^{as}CC$ and $\nu^{s}CC$ of pyridine and pyrrolidine rings, in accordance with the theoretical wavenumbers calculated for the main conformers (Table 4). Nonetheless, the theoretical–experimental match of VCD and IR spectra in DMSO is slightly worse than for the pure liquid and the CCl_4 solution, indicating that the solute–solvent interactions are higher than theoretically expected in this case. The determination of the solution-state conformer population of (−)-*S*-nicotine can be carried out taking the VCD spectra as a reference rather than the IR spectra.

Figures S7 and S8 (see the Supporting Information) show the IR and VCD spectral profiles calculated for theoretical m01/m02 conformational compositions ranging from 100% m01 to 100% m02 (i.e. 100% m01, 2:1, 1:1, 1:2 and 100% m02), compared with the experimentally recorded IR and VCD spectra. These figures show that, although the Boltzmann-averaged IR spectral profile obtained for different m01/m02 mixtures hardly differ (all of them being in rather good agreement with experiment), the experimental VCD spectral profile of the sample is only matched by the Boltzmann-averaged spectra calculated for a 2:1 m01/m02 composition (66.6% m01 and 33.3% m02). Thus, although the IR spectra of the sample can be rationalized by any of the conformational compositions (even pure m01 or m02), the spectral features observed in the VCD spectra of the sample can only be explained by the presence of both conformational configurations in a specific ratio (panel B in Figure S8).

Although FTIR is one of the most widespread techniques to determine the contribution of single conformers to the vibrational spectral profile of numerous types of samples, the (−)-S-

Table 4. VCD and IR bands observed experimentally for the pure liquid (−)-*S*-nicotine, CCl_4, and DMSO solutions, together with their corresponding theoretical band (B3LYP/aug-cc-pVTZ) and their proposed assignment.

	Experimental IR			VCD			Theoretical B3LYP/augTZ (unscaled)			
Peak	neat	CCl_4	DMSO	neat[a]	CCl_4[a]	DMSO[a]	m01 ($R_i\times10^{-44}$)[b]	m02 ($R_i\times10^{-44}$)[b]	NMV[c]	Assignment
P1	1476	1477	1477	1478 (−)	1476 (−)	1477 (−)	1513 (+0.5)	1511 (−12.5)	$\delta_{ip}CH_{pyr}+scCH_2$	m01 + m02
							1509 (−10.1)	1509 (+1.6)		
							1501 (+2.0)	1501 (+0.6)	pCH_3	m01 + m02
P2	1457	1457	1457	1457 (−)	1457 (−)	1455 (−)	1494 (−7.8)	1494 (−7.9)	$\delta^{as}CH_3+scCH_2$	m01 + m02
							1492 (−1.5)	1492 (−1.6)		
P3	–	–	–	1429 (+)	1428 (+)	1429 (+)	1465 (+15.2)	1465 (+15.1)	$\delta_{ip}CH_{PY}+\delta^{s}CH_3$	m01 + m02
P4	1427	1428	-	1422 (+)	1422 (+)	1424 (+)	1455 (+6.0)	1454 (+6.7)	$\delta^{s}CH_3+\delta_{ip}CH_{PY}$	m01 + m02
P5	1415	1416	-	1361 (−)	1360 (−)	1362 (−)	1397 (−11.5)	1396 (−10.0)	$\delta_{ip}CH_{PY}+waCH_2$	m01 + m02
P6	1361	1362	1364	1342 (+)	1343 (+)	1337 (+)	1379 (+4.7)	1379 (+8.1)	$waCH_2$	m01 + m02
							1353 (−3.8)	1355 (−3.9)	$\delta_{ip}CH_{PY}+waCH_2$	m01 + m02
P7	1342	1342	1342	1328 (+)	1327 (+)	1328 (+)	1349 (+12.7)	1350 (+11.3)	$\delta_{ip}CH_{PY}+waCH_2$	m01 + m02
P8	–	–	–	1321 (−)	1321 (−)	1321 (−)	1326 (−2.0)	1325 (−1.0)	$waCH_2$	m01 + m02
P9	1314	1314	1315	1312 (+)	1312 (+)	1311 (+)	1301 (+9.9)	1301 (+9.8)	ρCH_2	m01 + m02
P10	1289	1289	1291	1289 (−)	1289 (−)	1288 (−)	1288 (−10.7)	1288 (−11.3)	$\rho CH_2+\nu CC_{PY}$	m01 + m02
P11	1245	1245	1246	1248 (−)	1248 (−)	1244 (−)	1281 (−2.8)	1276 (−5.4)	$\nu CC_{PY}+\rho CH_2+\rho CH_3$	m01 + m02
P12	1216	1218	1216	1220 (+)	1220 (+)	1221 (+)	1248 (+45.6)	1248 (+68.5)	$\rho Ch_2+\delta_{ip}CH_{PY}$	m01 + m02
							1245 (+2.5)			
P13	–	–	–	1209 (−)	1207 (−)	1210 (−)	1236 (−18.0)	1242 (−26.4)	$\delta_{ip}CH_{PY}+\rho CH_2$	m01 + m02
P14	–	–	–	1202 (−)	1199 (−)	1202 (−)	–	1228 (−34.6)	ρCH_2	m02
								1221 (−6.7)		
P15	1189	1190	1190	1189 (−)	1189 (−)	1193 (−)	1214 (−13.5)	–	$\rho CH_2+\rho CH_3+\nu CC_{pyr}$	m01
P16	–	–	–	1181 (−)	1183 (−)	–	1203 (−10.2)	1204 (+3.8)	$\delta_{ip}CH_{PY}+\rho CH_3$	m01 + m02
P17	1175	1176	1177	1175 (+)	1177 (+)	1178 (+)	1177 (−33.9)	1178 (−27.6)	$\nu N\text{-}CH_3+\rho CH_2+\rho CH_3$	m01 + m02
P18	1156	1155	1154	1157 (−)	1156 (−)	1156 (−)	1139 (−3.8)	1140 (−0.7)	ρCH_3	m01 + m02
P19	1128 (sh)	1128 (sh)		1133 (+)	1131 (+)	1137 (+)	1136 (+2.7)	1139 (−1.6)	$\delta_{ip}CH_{PY}$	m01 + m02
P20	1115	1116		1115 (−)	1117 (−)		1104 (+1.7)	1104 (+8.0)	$twCH_2+\nu CC_{pyr}$	m01 + m02
P21	1103	1103		1108 (+)	1107 (+)		1066 (+0.6)	1068 (+2.4)	$\delta_{ip}CH_{PY}+breath_{PY}$	m01 + m02
P22	1085	1088		1085 (+)	1085 (+)		1060 (+18.1)	1059 (+8.3)	$\rho CH_3+breath_{PY}$	m01 + m02
P23	1044	1046		1047 (+)	1044 (+)		1044 (−1.1)	1043 (+0.9)	$\delta_{ip}CC_{PY}$	m01 + m02
P24	1024	1026		1035(−)	1036 (−)		1028 (−1.6)	1027 (−3.9)	$\nu^{as}CC_{pyr}+breath_{PY}$	m01 + m02
P25	–	–		1019 (−)	1020 (−)		1020 (−0.5)	1015 (−0.03)	$\delta_{oop}CH_{PY}$	m01 + m02
P26	970	970		969 (+)	969 (+)		994 (+4.5)	995 (+8.0)	$\delta_{oop}CC_{PY}+\rho CH_2+\rho CH_3$	m01 + m02
							972 (−5.6)	968 (−1.1)	$\delta_{oop}CC_{PY}+\rho CH_2+\rho CH_3$	m01 + m02
P27	948	948		949 (−)	951 (−)		957 (+1.0)	963 (−2.3)	$\delta_{oop}CC_{PY}$	m01 + m02
P28	921	924		922 (−)	923 (−)		934 (−4.1)	936 (−4.2)	$\nu^{s}CC_{pyr}+breath_{PY}$	m01 + m02
P29	903	903		902 (+)	902 (+)		918 (+10.5)	917 (+13.3)	$\nu^{s}CC_{pyr}+breath_{PY}$	m01 + m02
							910 (+12.5)	912 (+11.2)		

[a] The sign of the peaks is shown in brackets. [b] Theoretical wavenumbers calculated for m01 and m02 conformers of (−)-*S*-nicotine in the gas phase at the B3LYP/aug-cc-pVTZ level (unscaled). Calculated rotational strengths (R_ix10^{-44}) in esu^{2}cm^2 are shown in brackets. All modes have A symmetry. [c] ν = stretching, δ = deformation, ρ = rocking, sc = scissoring, tw = twisting, wa = wagging, breath = breathing, sh = shoulder. Superscripts s and as denote symmetric and asymmetric motions. Superscripts ip and oop denote in plane and out-of-plane vibrational motions. Subscript PY stands for pyridine ring. Subscript pyr stands for pyrrolidine ring. The description of the vibrational modes is proposed by visual inspection using Gaussview 5.0.

nicotine molecule may be an example of a relatively constrained system for which the identification of unique configurations in its IR spectrum is difficult. This compound is present in two different conformations and there are only subtle differences in their molecular structures and their associated vibrational spectral features; 1250–1150 cm^{-1} is the region of interest for their discrimination. In this region, the experimental VCD spectra of the sample show the following features: P11 centered at 1248 cm^{-1} (−), P12 centered at 1220 cm^{-1} (+), P13 centered at 1209 cm^{-1} (−), P14 centered at 1202 cm^{-1} (−), P15 centered at 1189 cm^{-1} (−), P16 centered at 1181 cm^{-1} (−), and P17 centered at 1177 cm^{-1} (+). These features are reproduced well by the theoretical Boltzmann-averaged spectra calculated for the system (Figure 6). In contrast, the IR spectra of the sample in this region show only P11, P12, P15 and P17 peaks, centered at 1245 cm^{-1}, 1216 cm^{-1}, 1189 cm^{-1} and 1175 cm^{-1}, respectively (Figure 7).

Some of the experimental VCD features can be assigned to only one conformer and others can only be justified if both conformations are considered to be present in a specific ratio (Figure 6 and Table 4). Thus, in the sequence of peaks P12(+), P13(−), P14(−), P15(−), and P16(−), which is perfectly imitated by our theoretical results, peaks P13, P14, P15, and P16 are crucial to confirm the presence of conformer m02 in addition to the global minimum m01.

The position and the relative intensity of P13(−) can only be justified if both conformers are present in a 2:1 ratio. This band has been attributed to the $\delta_{ip}CH$ of the pyridine ring

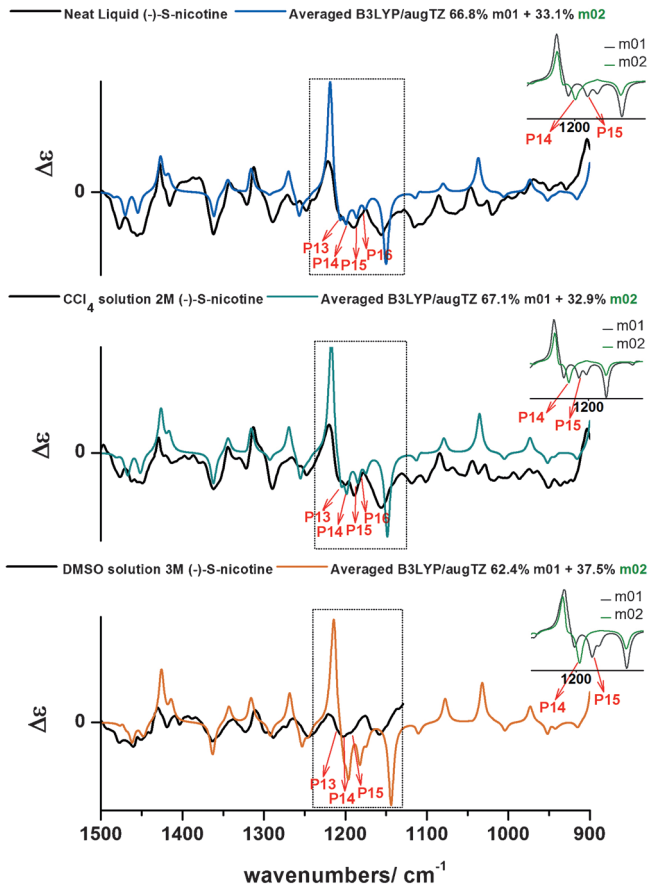

Figure 6. Experimental VCD spectra for (−)-*S*-nicotine compared with the predicted B3LYP/aug-cc-pVTZ Boltzmann-averaged spectra in the 1500–900 cm^{-1} region: Top) Neat liquid (black; resolution 4 cm^{-1}, 2000 scans, 6 μm)/Boltzmann-averaged (blue) spectra calculated in gas phase. Middle) CCl_4 solution (black; resolution 4 cm^{-1}, 2000 scans, 50 μm)/Boltzmann-averaged (green) spectra calculated in CCl_4. Bottom) DMSO solution (black; resolution 4 cm^{-1}, 2000 scans, 6 μm)/Boltzmann-averaged (orange) spectra calculated in DMSO. Boltzmann's populations at 298.15 K, full width at half maximum (FWHM) = 8 cm^{-1}. In the insets, we show the corresponding population-weighted theoretical spectra calculated for m01 (grey) and m02 (green) conformers of (−)-*S*-nicotine in the 1250–1150 cm^{-1} region.

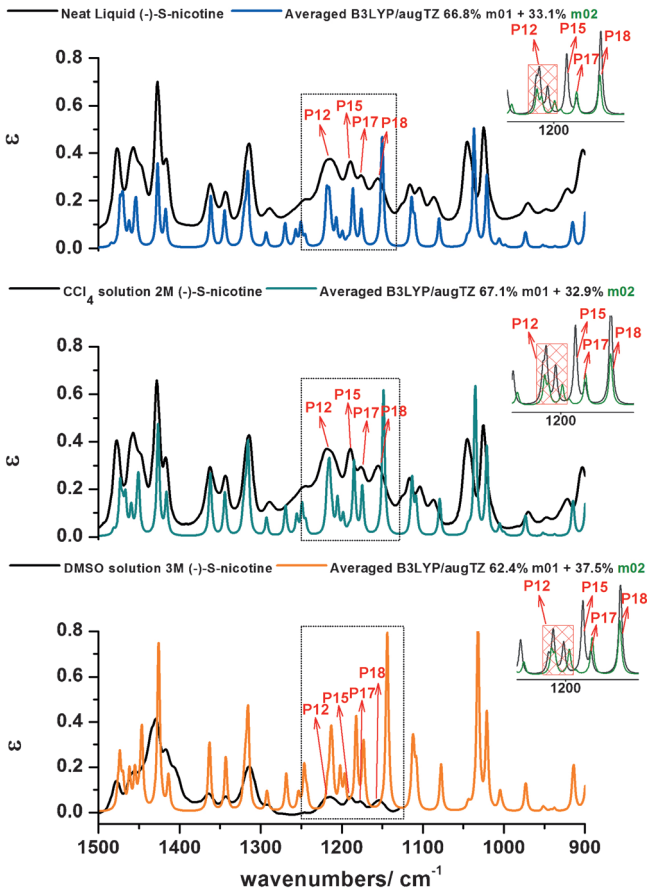

Figure 7. Experimental IR spectra for (−)-*S*-nicotine compared with the predicted B3LYP/aug-cc-pVTZ Boltzmann-averaged spectra in the 1500–900 cm^{-1} region: Top) Neat liquid (black; resolution 4 cm^{-1}, 2000 scans, 6 μm)/Boltzmann-averaged (blue) spectra calculated in gas phase. Middle) CCl_4 solution (black; resolution 4 cm^{-1}, 2000 scans, 50 μm)/Boltzmann-averaged (green) spectra calculated in CCl_4. Bottom) DMSO solution (black; resolution 4 cm^{-1}, 2000 scans, 6 μm)/Boltzmann-averaged (orange) spectra calculated in DMSO. Boltzmann's populations at 298.15 K, FWHM = 8 cm^{-1}. In the insets, we show the corresponding population-weighted theoretical spectra calculated for m01 (grey) and m02 (green) conformers of (−)-*S*-nicotine in the 1250–1150 cm^{-1} region.

combined with the ρCH_2 of the pyrrolidine ring in the m01 and m02 conformers. P14(−), centered at 1202 cm^{-1}, can only be assigned to the ρCH_2 of the pyrrolidine ring in m02 conformer, in accordance with its theoretical wavenumber; the theoretical spectrum of conformer m01 does not show any feature that could justify the experimental observation of P14 (see the top-right spectra in Figure 6). Similarly, P15(−), centered at 1189 cm^{-1}, is only attributable to the presence of conformer m01 (see insets in Figure 6). This band has been assigned to ρCH_2 and ρCH_3 combined with νCC of the pyrrolidine ring in the m01 conformer. Finally, the low intensity of P16 in the experimental VCD spectra can be explained by considering the theoretical Boltzmann-averaged VCD spectra of m01 and m02 conformers in a 2:1 ratio. As shown in Figure 6 and in Table 4, m01 and m02 conformers are calculated to have a peak centered at 1203 cm^{-1} and 1204 cm^{-1} with opposite signs: m01 is negative (-10×10^{-44} $esu^2\,cm^2$) and m02 is positive ($+4\times10^{-44}$ $esu^2\,cm^2$). Experimentally, we observed a weak negative peak centered at 1181 cm^{-1}, which can be understood by considering the theoretical relative intensity of this peak calculated for both conformers and the Boltzmann-averaged theoretical spectra calculated for the system (i.e. the experimental band is negative, given the larger amount of m01 present in the sample, and its weak character is due to the positive contribution of m02 conformer).

This region, which is vital to determine the solution-state conformer distribution of (−)-*S*-nicotine, is not so well-resolved by the IR data. P13, P14, and P16, which are key to confirming the presence of m02 in the sample, are not identified in the IR spectrum, because of broad bandwidths and overlapping (Figure 7). The broad bandwidth and high intensity of P12 and P15 in the experimental IR spectra mask P13, P14, and P16 (see the insets in Figure 7). Thus, although in theory it should be possible to identify the presence of m01 and m02 conform-

ers, the shape and width of the bands in the experimental infrared spectra does not enable this.

Therefore, here it has been proven that VCD spectroscopy can show subtle spectral features derived from slight structural changes that cannot be detected by using IR spectroscopy. Hence, VCD spectroscopy is valuable for performing structural studies and solution-state conformer determinations of chiral samples, as it provides more high-quality information to verify theoretical conformational compositions.

3. Conclusions

A double strategy comprising 1) a "direct" search following chemical intuition and 2) a Monte-Carlo based search by means of molecular mechanics methods, allowed a thorough analysis of the PES of (−)-*S*-nicotine. The good internal consistency of our conformational search is proven by the agreement between the results obtained by both approximations.

Although up to seven different conformations of (−)-*S*-nicotine are possible, only two of them (the *trans* structures) are populated in the gas phase. These conformations are m01 and m02 and differ only in the relative orientation of the pyridine ring. The NBO and AIM analysis of their electronic structures allowed us to conclude that hyperconjugative delocalizations (rather than electrostatic interactions or intramolecular hydrogen bonding) tip the conformational preference towards m01.

As in the gas phase, solution-state calculations under the IEF-PCM model using solvents of increasing polarity (CCl_4, DMSO, and D_2O), indicate that only the m01 and m02 conformers are populated in a ratio of 2:1.

Calculations and experiments in solution suggest that neither the structure nor the conformational energy profile of (−)-*S*-nicotine are strongly dependent on the medium. The small effect that the surrounding media has on the calculated molecular geometries and relative energies reinforces our assumption of the limited effect of electrostatic interactions in the conformational equilibrium in the system. This conclusion is reinforced by the results of the NBO and AIM calculations on the electronic structure of the two main conformers. These calculations also allow us to discard the possible incidence of intramolecular hydrogen bonding.

VCD spectra of (−)-*S*-nicotine have been recorded, analyzed, and assigned for the first time. A comparison of the experimental spectra obtained for the neat liquid and for its solutions in CCl_4 and DMSO, show that, as stated above, the conformational population distribution of the sample is not strongly dependent on the medium.

A combined theoretical–experimental approach was implemented to carry out the vibrational analysis of (−)-*S*-nicotine. Some statements can be addressed in this respect: 1) although the B3PW91 functional yields reasonably good results, B3LYP/aug-cc-pVTZ seems to reproduce the experimental VCD spectral profile of the sample better. 2) The use a continuum solvation model (IEF-PCM) is a fairly good approach to calculate VCD spectra for relatively non-interacting solvents (i.e. CCl_4); however, the implicit treatment of highly polar solvents (i.e. DMSO) yields poorer results regarding relative VCD intensities.

VCD allowed us to effectively determine the conformer distribution in (−)-*S*-nicotine. Theoretical Boltzmann-averaged spectra calculated for the system reproduce rather well the experimental profiles and confirm the experimental m01/m02 ratio to be close to 2:1.

Finally, we have proven the added value of the VCD technique, in relation to IR spectroscopy, to determine the conformational distribution of chiral samples having particularly low energy barriers and very subtle structural differences between conformers, such as in (−)-*S*-nicotine. Notably, the analysis of the FTIR spectroscopic data does not allow the same conclusions to be reached as when the VCD technique is used. This study has revealed that the VCD spectra of relatively constrained chiral systems can show subtle spectral features, due to smooth skeletal conformational changes in the mid-frequency region that cannot be found by using FTIR spectroscopy, and, hence, can provide more high-quality information to verify its conformational composition.

Acknowledgements

Authors thank Andalussian government for funding (FQM173) and the Centro de Instrumentación Científico Técnico (CICT) of the University of Jaén for instrumental facilities.

Keywords: circular dichroism · conformation analysis · density functional calculations · IR spectroscopy · tobacco alkaloids

[1] W. C. Evans in *Trease and Evans Pharmacognosy, 16th ed.* (Ed.: P. Graham), Saunders Elsevier, Edinburgh, **2009**.
[2] a) R. Kluger in *Ashes to Ashes: America's Hundred-Years Cigarret War, The Public Health and the Unabashed Triumph of Philip Morris* (Ed.: A. A. Knopf), Vintage Books, New York, **1996**; b) M. Sapori in *Neuronal Nicotinic Receptors: Pharmacology and Therapeutic Opportunities* (Eds.: S. P. Arneric, J. D. Brioni), Wiley – Liss, New York, **1998**.
[3] M. Hadjiconstantinou, N. H. Neff, *Neuropharmacology* **2011**, *60*, 1209.
[4] N. L. Benowitz, *N. Engl. J. Med.* **2010**, *362*, 2295.
[5] A. W. Bannon, M. W. Decker, M. W. Holladay, P. Curzon, D. Donnelly-Roberts, P. S. Puttfarcken, R. S. Bitner, A. Diaz, A. H. Dickenson, R. D. Porsolt, M. Williams, S. P. Arneric, *Science* **1998**, *279*, 77.
[6] R. M. Elgen, J. C. Hunter, A. Dray, *Trends Pharmacol. Sci.* **1999**, *20*, 337.
[7] H. Yuan, P. A. Petukhov, *Bioorg. Med. Chem.* **2006**, *14*, 7936.
[8] C. Calloe, R. Goodrow, S. P. Olesen, C. Antzelevitch, J. M. Cordeiro, *Am. J. Physiol. Heart Circ. Physiol.* **2013**, *305*, H66.
[9] A. Kucinski, S. Wersinger, E. K. Stachowiak, M. Radell, R. Hesse, T. Corso, M. Parry, M. Bencherif, K. Jordan, S. Letchworth, M. K. Stachowiak, *Health* **2012**, *4*, 1178 and references therein).
[10] M. N. Tiwari, S. Agarwal, P. Bhatnagar, N. K. Singhal, S. K. Tiwari, P. Kumar, L. K. S. Chauhan, D. K. Patel, R. K. Chaturvedi, M. P. Singh, K. C. Gupta, *Free Radical Biol. Med.* **2013**, *65*, 704 and references therein.
[11] G. Anderson, M. Maes, *CNS Neurol. Disord. Drug Targets* **2014**, *13*, 137 and references therein
[12] P. A. Crooks, M. Li, L. P. Dwoskin, *Drug Metab. Dispos.* **1997**, *25*, 47.
[13] R. J. Radna, D. L. Beveridge, A. L. Bender, *J. Am. Chem. Soc.* **1973**, *95*, 3831.
[14] L. B. Kier, *Mol. Pharmacol.* **1968**, *4*, 70.
[15] B. Pullman, P. Courrière, J. L. Coubeils, *Mol. Pharmacol.* **1971**, *7*, 397.
[16] M. Berthelot, M. Decouzon, J. F. Gal, C. Laurence, J. V. Le Questel, P. C. Maria, J. Tortajada, *J. Org. Chem.* **1991**, *56*, 4490.
[17] D. E. Elmore, D. A. Dougherty, *J. Org. Chem.* **2000**, *65*, 742.
[18] J. Graton, M. Berthelot, J. F. Gal, S. Girard, C. Laurence, J. Lebreton, J. Y. Le Questel, P. C. Maria, P. Naus, *J. Am. Chem. Soc.* **2002**, *124*, 10552.

[19] T. Takeshima, R. Fukumoto, T. Egawa, S. Konata, *J. Phys. Chem. A* **2002**, *106*, 8734.
[20] M. Mora, M. E. Castro, A. Niño, F. J. Melendez, C. Muñoz-Caro, *Int. J. Quantum Chem.* **2005**, *103*, 25.
[21] T. Yoshida, W. A. Farone, S. S. Xantheas, *J. Phys. Chem. B* **2014**, *118*, 8273.
[22] F. Egidi, J. Bloino, C. Cappelli, V. Barone, *Chirality* **2013**, *25*, 701.
[23] C. Eddy, C. Roland, A. Eisner, *Anal. Chem.* **1954**, *26*, 1428.
[24] E. Wada, K. Yamasaki, M. Lida, K. Saito, Y. Nakayama, *Kenkyu Hokoku – Nippon Senbai Kosha Chuo Kenkyusho* **1957**, *97*, 27.
[25] M. Deželić, B. Nikolin, *Spectrochim. Acta Part A* **1967**, *23*, 1149.
[26] M. Seydou, G. Gregoire, J. Liquier, J. Lemaire, J. P. Schermann, C. Desfrançois, *J. Am. Chem. Soc.* **2008**, *130*, 4187.
[27] M. Baranska, J. C. Dobrowolski, A. Kaczor, K. Chruszcz-Lipska, K. Gorz, A. Rygula, *J. Raman Spectrosc.* **2012**, *43*, 1065.
[28] J. U. Grabow, S. Mata, J. L. Alonso, I. Pena, S. Blanco, J. C. López, C. Cabezas, *Phys. Chem. Chem. Phys.* **2011**, *13*, 21063.
[29] P. S. Hammond, Y. Wu, R. Harris, T. J. Minehardt, R. Car, J. D. Schmitt, *J. Comput.-Aided Mol. Des.* **2005**, *19*, 1.
[30] P. J. Stephens, F. J. Devlin, J. R. Cheeseman in *VCD Spectroscopy for Organic Chemists*, CRC, Boca Raton, **2012**, Chap. 2: The experimental measurement of Vibrational Absorption and Vibrational Circular Dichroism Spectra.
[31] T. Kuppens, *Development of methodology to assign absolute configurations using Vibrational Circular Dichroism*, Dissertation for the degree of Doctor in Sciences, Ghent University (Belgium), December **2006**.
[32] T. A. Halgren, *J. Comput. Chem.* **1996**, *17*, 490.
[33] T. A. Halgren, *J. Comput. Chem.* **1996**, *17*, 520.
[34] T. A. Halgren, *J. Comput. Chem.* **1996**, *17*, 553.
[35] T. A. Halgren, R. B. Nachbar, *J. Comput. Chem.* **1996**, *17*, 587.
[36] T. A. Halgren, *J. Comput. Chem.* **1996**, *17*, 616.
[37] M. Clark, R. D. Cramer, N. V. Opdensch, *J. Comput. Chem.* **1989**, *10*, 982.
[38] SPARTAN'08, Wavefunction, Inc. Irvine, CA, Y. Shao, L. F. Molnar, Y. Jung, J. Kussmann, C. Ochsenfeld, S. T. Brown, A. T. B. Gilbert, L. V. Slipchenko, S. V. Levchenko, D. P. O'Neill, R. A. DiStasio Jr., R. C. Lochan, T. Wang, G. J. O. Beran, N. A. Besley, J. M. Herbert, C. Y. Lin, T. Van Voorhis, S. H. Chien, A. Sodt, R. P. Steele, V. A. Rassolov, P. E. Maslen, P. P. Korambath, R. D. Adamson, B. Austin, J. Baker, E. F. C. Byrd, H. Dachsel, R. J. Doerksen, A. Dreuw, B. D. Dunietz, A. D. Dutoi, T. R. Furlani, S. R. Gwaltney, A. Heyden, S. Hirata, C.-P. Hsu, G. Kedziora, R. Z. Khalliulin, P. Klunzinger, A. M. Lee, M. S. Lee, W. Z. Liang, I. Lotan, N. Nair, B. Peters, E. I. Proynov, P. A. Pieniazek, Y. M. Rhee, J. Ritchie, E. Rosta, C. D. Sherrill, A. C. Simmonett, J. E. Subotnik, H. L. Woodcock, W. Zhang, A. T. Bell, A. K. Chakraborty, D. M. Chipman, F. J. Keil, A. Warshel, W. J. Hehre, H. F. Schaefer, J. Kong, A. I. Krylov, P. M. W. Gill, M. Head-Gordon, *Phys. Chem. Chem. Phys.* **2006**, *8*, 3172.
[39] Gaussian 09 (Revision D.01), M. J. Frisch, G. W. Trucks, H. B. Schlegel, G. E. Scuseria, M. A. Robb, J. R. Cheeseman, G. Scalmani, V. Barone, B. Mennucci, G. A. Petersson, H. Nakatsuji, M. Caricato, X. Li, H. P. Hratchian, A. F. Izmaylov, J. Bloino, G. Zheng, J. L. Sonnenberg, M. Hada, M. Ehara, K. Toyota, R. Fukuda, J. Hasegawa, M. Ishida, T. Nakajima, Y. Honda, O. Kitao, H. Nakai, T. Vreven, J. A. Montgomery, Jr., J. E. Peralta, F. Ogliaro, M. Bearpark, J. J. Heyd, E. Brothers, K. N. Kudin, V. N. Staroverov, T. Keith, R. Kobayashi, J. Normand, K. Raghavachari, A. Rendell, J. C. Burant, S. S. Iyengar, J. Tomasi, M. Cossi, N. Rega, J. M. Millam, M. Klene, J. E. Knox, J. B. Cross, V. Bakken, C. Adamo, J. Jaramillo, R. Gomperts, R. E. Stratmann, O. Yazyev, A. J. Austin, R. Cammi, C. Pomelli, J. W. Ochterski, R. L. Martin, K. Morokuma, V. G. Zakrzewski, G. A. Voth, P. Salvador, J. J. Dannenberg, S. Dapprich, A. D. Daniels, O. Farkas, J. B. Foresman, J. V. Ortiz, J. Cioslowski, D. J. Fox, Gaussian, Inc., Wallingford CT, **2013**.
[40] A. D. Becke, *J. Chem. Phys.* **1993**, *98*, 5648.
[41] C. Lee, W. Yang, R. G. Parr, *Phys. Rev. B* **1988**, *37*, 785.
[42] J. P. Perdew, J. A. Chevary, S. H. Vosko, K. A. Jackson, M. R. Pederson, D. J. Singh, C. Fiolhais, *Phys. Rev. B* **1992**, *46*, 6671.
[43] P. Perdew, K. Burke, Y. Wang, *Phys. Rev. B* **1996**, *54*, 16533.
[44] J. F. Dobson, G. Vignale, M. P. Das, *Electronic Density Functional Theory: Recent Progress and New Directions*, Plenum, Springer US, New York, **1998**.
[45] A. D. McLean, G. S. Chandler, *J. Chem. Phys.* **1980**, *72*, 5639.
[46] R. A. Kendall, T. H. Dunning, Jr., R. J. Harrison, *J. Chem. Phys.* **1992**, *96*, 6796.
[47] P. J. Stephens, F. J. Devlin, J. R. Cheeseman in *VCD Spectroscopy for Organic Chemists*, CRC, Boca Raton, **2012**, Chapter. 4: Ab Initio Methods; Chapter 5: Analyses of the IR and VCD Spectra of Conformationally Rigid Molecules.
[48] J. S. Binkley, J. A. Pople, *Int. J. Quantum Chem.* **1975**, *9*, 229.
[49] G. A. Petersson, A. Bennett, T. G. Tensfeldt, M. A. Al-Laham, W. A. Shirley, J. Mantzaris, *J. Chem. Phys.* **1988**, *89*, 2193.
[50] G. A. Petersson, M. A. Al-Laham, *J. Chem. Phys.* **1991**, *94*, 6081.
[51] A. E. Reed, L. A. Curtiss, F. Weinhold, *Chem. Rev.* **1988**, *88*, 899.
[52] E. D. Glendening, J. K. Badenhoop, A. E. Reed, J. E. Carpenter, J. A. Bohmann, C. M. Morales, C. R. Landis, F. Weinhold, NBO *v. 6.0*. Theoretical Chemistry Institute, University of Wisconsin, Madison, WI, USA, **2013**.
[53] F. W. Biegler-König, J. Schönbohm, *J. Comput. Chem.* **2002**, *23*, 1489.
[54] F. Biegler-König and J. Schönbohm, AIM2000 *v. 2*, University of Applied Sciences, Bielefeld, Germany, **2000**.
[55] S. Miertuš, E. Scrocco, J. Tomasi, *Chem. Phys.* **1981**, *55*, 117.
[56] J. Tomasi, B. Mennucci, R. Cammi, *Chem. Rev.* **2005**, *105*, 2999.
[57] B. Mennucci, E. Cances, J. Tomasi, *J. Phys. Chem. B* **1997**, *101*, 10506.
[58] E. Cancès, B. Mennucci, J. Tomasi, *J. Chem. Phys.* **1997**, *107*, 3032.
[59] E. Cancès, B. Mennucci, *J. Math. Chem.* **1998**, *23*, 309.
[60] C. Altona, M. Sundaral, *J. Am. Chem. Soc.* **1977**, *59*, 1211.
[61] A. Pedretti, L. Villa, G. Vistoli, *J. Mol. Graphics* **2002**, *21*, 47.
[62] A. Pedretti, L. Villa, G. Vistoli, *Theor. Chem. Acc.* **2003**, *109*, 229.
[63] A. Pedretti, L. Villa, G. Vistoli, *J. Comput.-Aided Mol. Des.* **2004**, *18*, 167.
[64] V. P. Nicu, E. J. Baerends, *Phys. Chem. Chem. Phys.* **2009**, *11*, 6107.
[65] V. P. Nicu, E. Debie, W. Herrebout, B. Van der Veken, P. Bultinck, E. J. Baerends, *Chirality* **2009**, *21*, E287.

Received: September 19, 2014
Published online on November 24, 2014